Appl Phys B (2011) 104:951–956
DOI 10.1007/s00340-011-4390-x

Applied Physics B
Lasers and Optics

Filament-induced self-written waveguides in glassy $As_4Ge_{30}S_{66}$

I. Blonskyi · V. Kadan · O. Shpotyuk · M. Iovu · P. Korenyuk · I. Dmitruk

Received: 26 November 2010 / Revised version: 11 January 2011 / Published online: 8 February 2011

Abstract The filamentation of femtosecond laser pulses and filament-induced self-writing of a permanent waveguide are observed in $As_4Ge_{30}S_{66}$ chalcogenide glass. The radial profile of the self-written waveguide is extracted from the defocused transmission microscopic images via a two-step procedure: at first the phase image of the waveguide is computed using the transport-of-intensity equation and then the index profile is obtained from the phase image by applying the inversed Abel transform.

1 Introduction

Wide IR-transparency and high nonlinear refractive index of Chalcogenide Glasses (ChGs) define their great potential for photonics [1–4]. One remarkable property of ChGs is their photosensitivity which is caused by high steric flexibility typical to a low-coordinated network and relatively high intrinsic free volume frozen near the glass transition.

On the other hand, laser light is known to be an effective tool for fabrication of various embedded photonic structures in ChGs. It modifies their optical properties with high precision taking advantage of the enhanced photosensitivity of these materials. The successful inscribing of waveguides, optical couplers, diffraction gratings, all-optical switches [5] as well as the fabrication of 3D storage devices [2, 3] with femtosecond laser pulses has been reported recently both in bulk and film ChGs.

A number of significant advantages of the femtosecond lasers over traditional laser sources have been clearly demonstrated for these applications. However, the propagation of femtosecond laser pulses in and their interaction with the transparent materials differs significantly from that of pico- or nanosecond pulses, thus stimulating considerable interest of the researchers to the subject.

The waveguides can be directly inscribed in glassy As_2S_3 via translation of the sample along the tightly focused beam of the femtosecond laser oscillator, as described in [6]. A region of the reduced refractive index n ($\Delta n \sim -0.9 \times 10^{-3}$) was formed on the axis of the waveguide, surrounded by an area of increased n ($\Delta n \sim 0.2 \times 10^{-3}$). At the same time, the researchers report most often the positive index change in As_2S_3 caused by the femtosecond laser exposure. The single-channel waveguides and Y-couplers, featuring positive $\Delta n > 10^{-2}$ have been fabricated in 1.6-μm-thick As_2S_3 films using Ti:sapphire laser oscillator [3]. The exposure of the bulk As_2S_3 and thin film As_2S_3 samples to the femtosecond laser radiation at 800 nm resulted in a positive change of the refractive index as a result of photo darkening [7, 8].

Besides the direct writing, waveguides can also be produced by taking advantage of the self-writing effect. Indeed,

I. Blonskyi · V. Kadan (✉) · P. Korenyuk · I. Dmitruk
Dept. of Photonic Processes, Institute of Physics of National Academy of Sciences of Ukraine, 46, Prospect Nauky, Kyiv, 03680, Ukraine
e-mail: kadan@iop.kiev.ua

O. Shpotyuk
Lviv Scientific Research Institute of Materials of Scientific Research Company "Carat", 202, Stryiska Str., Lviv, 79031, Ukraine
e-mail: shpotyuk@novas.lviv.ua

O. Shpotyuk
Institute of Physics of Jan Dlugosz University, 13/15, al. Armii Krajowej, Czestochowa, 42201, Poland

M. Iovu
Center of Optoelectronics, Institute of Applied Physics of AS of Moldova, 1, Academiei str., Chisinau, 2028, Moldova
e-mail: miovu@asm.md

the appearance of waveguide channels is expected in photosensitive material if the positive refractive index change occurs under the laser exposure [9]. Light-induced self-writing effect was reported in Ce-doped glassy Ga-La-S [10] with 650 mW CW laser light at 1047 nm. The narrowing of the laser beam spot from 200 to 125 µm was observed after 1.5-hour exposure. No waveguide occurred, however, despite the increase of refractive index $\Delta n \sim 2.5 \times 10^{-4}$.

The femtosecond laser pulses seem to be more suitable for the waveguide self-writing because of their ability to form filaments, i.e., the long-distance propagation mode characterized by a narrow (few µm diameter in solids) and intense ($\sim 10^{13}$ W/cm^2) ionized core which contains a part ($\sim$10%) of the whole pulse energy. Unlike the Gaussian beams, the diameter of the filament core may persist for many diffraction lengths [11, 12]. A balance between two effects governs the filamentation: the optical Kerr effect (that induces an instant and reversible positive change of the refractive index, i.e., leads to self-focusing) and the generation of plasma in the intense filament core by the multiphoton absorption that causes a negative change, i.e., leads to self-defocussing. See, e.g., [11] for a filamentation review where both theoretical modeling and experiments are presented. The other consequence of the ionization apart from the fast filamentation can be the accumulation of the structural changes of the material in the filament core, enabling formation of the permanent waveguide. The successful filament-induced self-writing of the waveguides in oxide glasses involving this mechanism was reported in [13–15]. In contrast to the direct-writing technique, the self-writing is a one-step process, for which no translation of the sample is required. This ensures a better optical quality of the produced structure.

The filament-induced waveguides have not yet been recorded however in such an important class of materials, as ChGs, because the strong two-photon absorption (2PA), inherent to these mostly narrow-gap materials, prevents from filament formation.

The purpose of our work is to achieve the femtosecond filamentation and filament-induced waveguide self-writing in bulk ChG. With that end in view, a comparatively wide-gap ChG composition $As_4Ge_{30}S_{66}$ minimizing 2PA has been prepared. The bulk samples were used for the experiments keeping in mind the prospects of fabrication of three-dimensional structures. The appearance of the reversible Kerr filaments under the femtosecond laser excitation in this material has been recently detected by the authors for the first time in [16]. Here, we continue the study of the Kerr filamentation in glassy $As_4Ge_{30}S_{66}$, focusing on the filament-induced permanent modifications of the glass properties. At longer exposures, the self-writing of the permanent waveguide is observed, as a result of the structural transformation of the material in the filament core. The refractive index profile $\Delta n(r)$ of the waveguide is extracted then from a series of microscopic images by using Transport-of-Intensity Equation (TIE) and inverse Abel transform. The shape of the index profile allows for conclusion about densification of the material that occurs at the waveguide axis.

The paper is organized as follows: in Sect. 2 we provide a preparation procedure of the experimental samples; experimental setup is described in Sect. 3; Sect. 4 contains two main parts: at first we provide experimental results obtained under the femtosecond laser excitation, and finally we characterize the permanent waveguides ex situ using ordinary transmission microscopy and numerical calculations.

2 Glass synthesis and samples preparation

Bearing in mind that wide bandgap materials are needed for filamentation with 800 nm light, the glassy $As_4Ge_{30}S_{66}$ has been synthesizes that belongs to Ge-enriched composition within quasi-binary GeS_2-As_2S_3 cut-section (the germanium disulfide GeS_2 content reaching as high as 93.75 mol.%). The role of As_2S_3 additives is to suppress strong crystallization processes ensuring a good melt-quenching ability, since the stochiometric GeS_2 is too close to the border of glass-forming region [17, 18]. In contrast to g-As_2S_3, the structure of g-$As_4Ge_{30}S_{66}$ is more complex, being presented by a mixture of corner- and edge-sharing $GeS_{4/2}$ tetrahedrons interlinked with $AsS_{3/2}$ pyramids, most probably, with no direct Ge-As covalent bonds [17–19]. As a result, this glass with the average coordination number of $Z = 2.64$ (the mean number of covalent bonds per one atom within glass-forming structural unit) possesses a stressed and rigid backbone with more than 3.0 Lagrangian constraints per atom. The g-$As_4Ge_{30}S_{66}$ is a thermally stable material. Its characteristic T_g value is close to 700 K, and optical band-gap $E_g \approx 3.0$ eV [19, 20]. So, $E_g/h\nu$ ratio is 1.94 for 800 nm femtosecond laser pulses, which allows us to expect a weaker 2PA than in most ChGs.

The glassy samples of $As_4Ge_{30}S_{66}$ have been prepared by a conventional melt-quenching route [17, 18]. A mixture of high-purity initial compounds was melted in evacuated silica ampoules placed in a rocking furnace. The ingots were air-quenched to a glassy state, which was controlled both visually by a characteristic conch-like fracture surface, and by data of X-ray diffraction. Then the ingots were cut into rectangular slabs of $3 \times 3 \times 15$ mm dimensions and optically finished. To remove the mechanical strains that remain after quick cooling, the freshly quenched samples were additionally annealed near the glass transition temperature.

The refractive index n of g-$As_4Ge_{30}S_{66}$ at 800 nm determined from linear transmission measurements of a 0.5 mm thick slab accounting for multiple Fresnel reflections was estimated as $\sim$2.2.

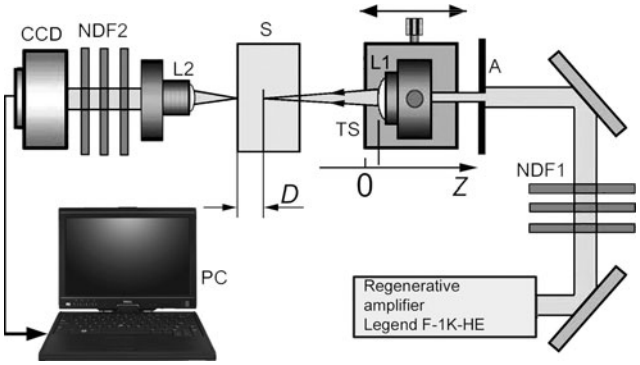

Fig. 1 Schematic diagram of the experimental set-up

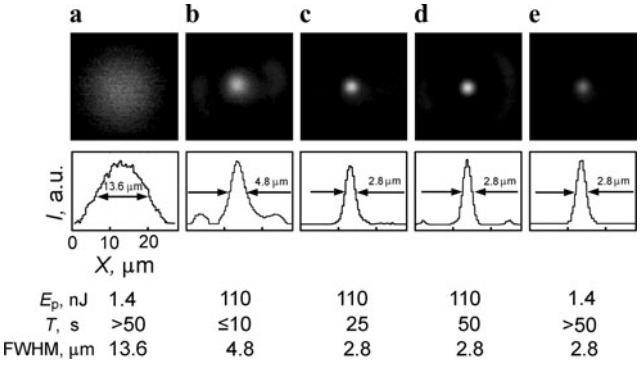

Fig. 2 The cross-sections and intensity profiles of the beam at the output face of the sample. The pulse energy E_p (nJ), exposure T (s), and beam FWHM (μm), are shown below the each fragment

3 Experimental

One of the possible ways to visualize directly the traveling laser pulse in wide-bandgap oxide glasses is the Femtosecond Time-resolved Optical Polarigraphy (FTOP) [21, 22]. In case of ChG samples, the residual optical anisotropy unfortunately prohibits the use of FTOP. Hence, in the experiment, we record the time-integrated near-field profiles of the beam at the exit face of the sample.

The experimental set-up is shown in Fig. 1. The regenerative amplifier delivers a train of 150 fs horizontally polarized pulses with 1000 s^{-1} repetition rate and 2.5 mJ pulse energy at 800 nm. The pulse energy can be adjusted with a set of calibrated neutral density filters NDF1. The aperture A cuts out a 2 mm diameter beam, which enters the lens L1 ($3.7\times/0.11$ NA). The lens L1 is mounted on the translation stage TS, which shifts the beam focal spot along the Z-axis inside the 3 mm thick sample S. We take as $Z = 0$ such a position of the translation stage at which the focal spot in linear propagation mode (no self-focusing) is on the back face of the sample. Note that the actual distance D between the focal spot position and the back face of the sample is $2.2Z$, taking into account the refractive index of the sample material. The distance between the aperture A and the lens L1 is 10 cm at $Z = 0$. The lens L2 ($10\times/0.25$ NA) images the outgoing beam from the back face of the sample on the matrix of the monochrome CCD-camera (1200 × 1600 pixels of 4.4 × 4.4 μm size). The spatial resolution of the imaging setup is approximately 2 μm. A set of neutral density filters NDF2 attenuates the beam intensity to avoid saturation of the CCD-camera.

4 Results and discussion

The beam intensity patterns at the output face of the sample and the intensity profiles taken at the translation stage position $Z = 0.2$ mm are presented in Fig. 2 for different pulse energies E_p, different exposures, and $D = 0.44$ mm. At $E_p = 1.4$ nJ, the beam profile is nearly Gaussian with 13.6 μm FWHM. The linear propagation mode is assumed as no dependence of the beam diameter on E_p and exposure time was observed for $E_p \leq 1.4$ nJ under exposures up to 20 minutes. Qualitatively different is the behavior for nonlinear beam propagation. With the increasing pulse energy its diameter strongly decreases down to 4.8 μm at $E_p = 110$ nJ. At short exposures $T \leq 10$ s, the process is reversible, i.e., the reset of E_p to the original value of 1.4 nJ, restores the original 13.6 μm beam diameter. It is important that in contrast to the linear propagation mode (a), at $E_p = 110$ nJ the beam diameter is not stable but depends on T. It decreases down to 2.8 μm at $T = 25$ s and retains this value at $T = 50$ s ((c) and (d)). In that case, the beam keeps 2.8 μm diameter even after the decrease of E_p to the initial value of 1.4 nJ (e). Thus, it can be concluded, that at $E_p = 110$ nJ and $T \geq 25$ s, the local optical properties of the sample become modified irreversibly. We do not mean a complete irreversibility here, as a slow natural aging processes proper to ChGs can erase the local structural transformation within the time range of several years [23].

The observed changes of the beam shape can be attributed to the self-focusing. At the beginning of exposure (b), only the fast Kerr self-focusing is important; therefore, the beam diameter follows in a reversible manner all changes of E_p. On the other hand, the local changes of the glass structure are triggered by the 2PA at the sufficiently high light intensity, being accumulated with the exposure time [3, 24–26]. These structural changes manifest themselves optically as the local rise of the refractive index with the maximum on the beam axis. The accumulated index changes act as a gradient lens; they become high enough at $T = 25$ s giving rise to the additional beam narrowing. It should be taken into account here that the femtosecond filament and permanent waveguide may also be formed in the sample. However, the described experiment is insufficient for unambiguous conclusion. Indeed, it is well known that a characteristic feature of the filament is the length of its

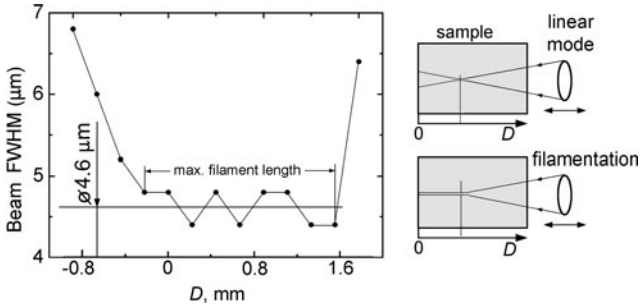

Fig. 3 Output beam diameter versus the distance D between the focal spot in linear mode and the back face of the sample

narrow core that far exceeds the Rayleigh diffraction length. The next measurement is intended to prove the appearance of the Kerr filamentation under the above experimental conditions. The diameter of the outgoing beam has been measured at different D to find the length of its narrow core in nonlinear mode at $E_p = 110$ nJ. The repetition rate has been reduced from 1000 to 25 pulses per second to prevent accumulation of the permanent index change and further beam narrowing during the measurements.

The results are shown in Fig. 3. It is seen that the beam diameter keeps its minimum value of 4.6 μm, oscillating by ±0.2 μm (half pixel size) within the D-range from −0.2 mm to 1.6 mm. The largest length of the narrow beam core inside the sample proves to be about 1.8 mm, thus far exceeding the Rayleigh diffraction length $z_R = 130$ μm for the Gaussian beam of 4.6 μm waist. The attenuation of E_p to 1.4 nJ by additional NDFs, leads to the strong widening of the outgoing beam. These data show that at $E_p = 110$ nJ and D within the range between −0.2 to 1.6 mm the filament of ∼1.8 mm maximum length is formed. It starts about 0.2 mm before the focal spot for linear propagation and ends up on the output face of the sample. The reversibility of the beam diameter under small exposures ($T \leq 400$ s at 25 s^{-1} and $T \leq 10$ s at 1000 s^{-1} repetition rates) observed in both the present and the previous experiments, indicates that the filamentation at the first stage is governed by fast Kerr nonlinearity. The permanent changes of the refractive index dominate at $T \geq 25$ s (1000 s^{-1}), producing a waveguide which is capable to guide a low-intensity light in the linear mode. Therefore, after the long enough exposures, the decrease of E_p to 1.4 nJ does not result in increase of the outgoing beam diameter (Fig. 2(e)). Evidently, the increase of the permanent refractive index after such exposure is high enough to capture and guide a low-intensity beam, despite negligible Kerr contribution to the beam focusing.

The self-writing of filament-induced permanent waveguides in wide-gap transparent solids has already been reported in [13–15]. The observation of this phenomenon in ChG becomes possible because a relatively wide-gap composition has been synthesized, with the reduced 2PA. In this way, the main factor which prevents the femtosecond filamentation in more narrow-gap ChGs has been weakened.

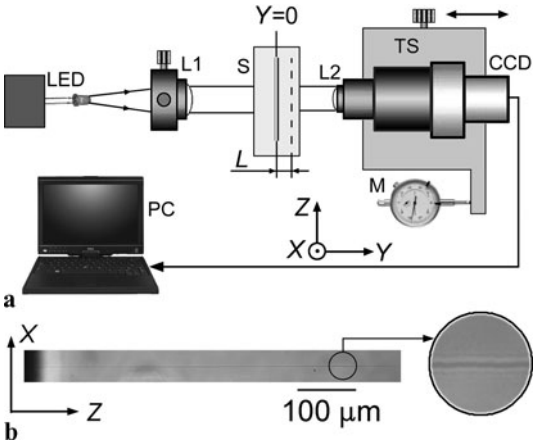

Fig. 4 (**a**) Schematic view of the microscopy set-up. (**b**) Microscopic picture of the fragment of filament-induced optical waveguide in bulk g-$As_4Ge_{30}S_{66}$, taken at $L = -10$ μm using 10× lens

The low-intensity CW laser radiation which does not form filaments can, however, induce the self-written waveguides in photosensitive media too, as mentioned above. The main physical reason for such self-writing is the accumulation of light-induced refractive index change Δn under the laser exposure [10]. We believe that two principal mechanisms are involved in the waveguide formation in our present experiment. At first, the Kerr filament develops, while the permanent waveguide occurs later as a consequence of the gradual increase of n on the filament axis. The latter process gives rise to the further beam narrowing caused by its self-trapping in the induced waveguide. Just this phenomenon is observed in our experiment, when the original 4.8 μm filament (Fig. 2(b)) shrinks to 2.8 μm after 25 s exposure (Fig. 2(c, d)). One possible physical reason for the permanent index change is the bond reconfiguration triggered by the 2PA-excited free carriers in the filament core [3, 24–26]. Thermal mechanism of the index change can also be involved in the permanent waveguide formation, taking into account the 2PA-caused energy deposition in the filament core. In this case, the glass parameters can be changed due to the diffusion of the components in the temperature gradient. The clarification of the exact mechanism of the index change is a subject of the further studies.

The characterization of permanent filament-induced waveguides in g-$As_4Ge_{30}S_{66}$ is described from now on. The sample S, previously exposed to the laser pulses during 50 s with $E_p = 110$ nJ and repetition rate 1000 s^{-1} at $Z = 0.4$ mm ($D = 0.88$ mm) in geometry shown in Fig. 1, has been examined using conventional optical microscopy (Fig. 4(a)). The beam of the red LED with maximum wavelength $\lambda_{max} = 630$ nm, which is collimated by the lens L1 ($F = 10$ cm), is used as a back-illumination source. The microscope lens L2 with the magnification 10× or 20×

projects the magnified image on the CCD matrix. The object plane is adjusted along the Y-axis with ± 0.5 µm accuracy, using the manual translating stage TS and micrometric dial indicator M.

Being purely phase object, the filament-induced waveguide is invisible in conventional optical microscopy if it lies exactly in the microscope object plane (position $Y = 0$ in Fig. 4(a)). An intensity pattern appears, on the contrary, in slightly defocused object plane ($Y = L$), what is caused by the interference of the waves deflected by the local refractive index gradients. Figure 4(b) shows a fragment of such an intensity pattern, that appears at $L = -10$ µm. It looks like a narrow "thread," buried in the bulk $As_4Ge_{30}S_{66}$ sample. The pump beam was directed from the right to the left along the Z-axis during the writing process. The boundary between the bright and dark areas at the left side of the picture is the position of the sample back face (in writing geometry, Fig. 1). The whole length of the observed structure (about 670 µm) exceeds the camera field of view. A fourfold magnified fragment of the structure is also shown in Fig. 4(b). Even the first glance at the photo suggests that the refractive index change at the axis of the written structure is positive. Indeed, it acts as a convex cylindrical lens, since the axial intensity exceeds background at $L > 0$, and vice versa at $L < 0$.

The technique of quantitative refractive shadowgraphy [27–29] is used to extract the actual profile of refractive index in the waveguide from its defocused shadowgram. At first, the phase image of the object is computed basing on the transport-of-intensity equation (TIE) [30]. It links the intensity and phase distribution while wave is propagating in the optically disturbed space in assumption of negligible diffraction at small defocussing values and purely phase objects. For the object slowly varying along Z-axis the TIE reads:

$$\frac{d^2}{dx^2}\left(\int_{-\Delta y}^{\Delta y} \Delta n(x, y)\, dy\right) = -\frac{I(x) - I_0}{L I_0}, \tag{1}$$

where I_0 stands for the illuminating beam intensity; $I(x)$ is the transverse intensity profile in the object plane lying at the distance L from the phase object; Δy is the half-thickness of the phase object; $\Delta n(x, y)$ is the refractive index variation. The phase image or, in other words, the variation of the optical path in the sample along the Y-axis which is due to the local change of the refractive index is represented by $F(x) = \int_{-\Delta y}^{\Delta y} \Delta n(x, y)\, dy$. The (1) has been integrated numerically using the measured intensity profile $I(x)$ of the waveguide fragment, shown in the inset in Fig. 5. Thus, the phase image $F(x)$ is reconstructed from the two transverse intensity patterns I_0 at $Y = 0$ and $I(x)$ at $Y = 10$ µm.

The final step involves the inverse 1D Abel transform in assumption of the cylindrical symmetry of the written waveguide [31]:

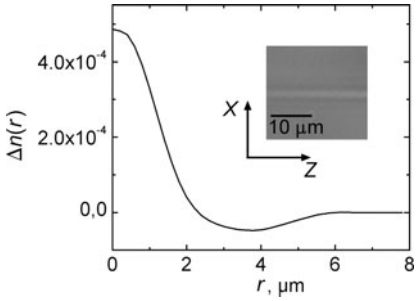

Fig. 5 Refractive index profile $\Delta n(r)$ of the waveguide. The *inset* shows a fragment of the microscopic picture of the waveguide, taken with 20× lens at $L = 10$ µm

$$\Delta n(r) = -\frac{1}{\pi}\int_r^R \frac{dF(x)}{dx}\frac{1}{\sqrt{R^2 - x^2}}\, dx. \tag{2}$$

Thus, the actual refraction index profile $\Delta n(r)$ is extracted from $F(x)$ (Fig. 5).

The profile presents nearly 3 µm-thick positive part with Δn up to 0.5×10^{-3} surrounded by a negative bouncing of ~7 µm diameter. Such a shape of the profile can be explained assuming the densification of the material on the waveguide axis, which necessarily leads to the increase of the refractive index. If that is the case, the densification on the axis is compensated by a surrounding zone of lower density and, hence, of lower index, just as is observed.

5 Summary

The self-writing of permanent waveguides induced by the filamentation of the femtosecond laser pulses is observed for the first time in ChGs, with g-$As_4Ge_{30}S_{66}$ as an example. The process of self-writing is shown to occur in two stages. At the first stage which is reversible, the filament forms as a result of the Kerr self-focusing, while the 2PA-caused ionization and heating of the material in the filament core trigger permanent structural transformation and irreversible change of refractive index. At the second stage which becomes apparent after the exposure of several tens of seconds, the build-up of the index change results in the formation of the permanent waveguide capable of guiding low-intensity light in the linear mode. The refractive index profile of the waveguide is reconstructed from its defocused microscopic images by using the transport-of-intensity equation and inverse Abel transform. The index profile features the positive index change up to 0.5×10^{-3} in the 3 µm-thick core, enveloped by a zone with negative index change of nearly 7 µm diameter. Such a profile suggests that the densification of the material is responsible for the axial increase of the index, while the tensile stress generates the area of decreased index around the core.

Acknowledgements The financial support from Science and Technology Center in Ukraine (project #3745), Ukrainian State Program "Nanotechnologies and Nanomaterials," and the Program of NAS of Ukraine "Fundamental Problems of Nanostructured Systems, Nanomaterials, and Nanotechnologies" is gratefully acknowledged.

References

1. A. Zakery, S.R. Elliott, *Optical Nonlinearities in Chalcogenide Glasses and Their Applications* (Springer, Berlin, Heidelberg, New York, 2007)
2. D.-Y. Choi, S. Madden, A. Rode, R. Wang, B. Luther-Davies, N.J. Baker, B.J. Eggleton, Opt. Express **15**, 7708 (2007)
3. A. Zoubir, M. Richardson, C. Rivero, A. Schulte, C. Lopez, K. Richardson, N. Ho, R. Vallee, Opt. Lett. **29**, 748 (2004)
4. K. Suzuki, Y. Hamachi, T. Baba, Opt. Express **17**, 22393 (2009)
5. J.M. Harbold, F.O. Ilday, F.W. Wise, J.S. Sanghera, V.Q. Nguyen, L.B. Shaw, I.D. Aggarwal, Opt. Lett. **27**, 119 (2002)
6. D. Le Coq, P. Masselin, Ch. Przygodsky, E. Bychkov, J. Non-Cryst. Solids **355**, 1832 (2009)
7. A. Zoubir, M. Richardson, C. Rivero, C. Lopez, N. Ho, R. Vallee, K.A. Richardson, OSA Trends Opt. Photonics **73**, 125 (2002)
8. O.M. Efimov, L.B. Glebov, K.A. Richardson, E. Van Stryland, T. Cardinal, S.H. Park, M. Couzi, J.L. Bruneel, J. Opt. Mater. **17**, 379 (2001)
9. T.M. Monro, C.M. de Sterke, I. Poladian, J. Opt. Soc. Am. B **13**, 2824 (1996)
10. A.M. Ljungstrom, T.M. Monro, J. Lightwave Technol. **20**, 78 (2002)
11. A. Couairon, A. Mysyrowicz, Phys. Rep. **441**, 47 (2007)
12. V.P. Kandidov, S.A. Shlenov, O.G. Kosareva, Quantum Electron. **39**, 205 (2009)
13. V. Kudriasov, E. Gaizauskas, V. Sirutkaitis, J. Opt. Soc. Am. B **22**, 2619 (2005)
14. D.G. Papazoglou, I. Zergioti, S. Tzortzakis, Opt. Lett. **32**, 2055 (2007)
15. I. Zergioti, K.D. Kyrkis, D.G. Papazoglou, S. Tzortzakis, Appl. Surf. Sci. **253**, 7865 (2007)
16. I. Blonskyi, V. Kadan, O. Shpotyuk, M. Iovu, I. Pavlov, Opt. Mater. **32**, 1553 (2010)
17. A. Feltz, *Amorphe und Glasartige Anorganishe Festkörper (Amorphous and Vitreous Inorganic Solids)* (Akademie-Verlag, Berlin, 1983)
18. Z.U. Borisova, *Chalcogenide Vitreous Glasses* (Leningrad Univ., Leningrad, 1982)
19. S. Onari, T. Inokuma, H. Kataura, T. Arai, Phys. Rev. B **35**, 4373 (1987)
20. A. Andriesh, M. Bertolotti (eds.), *Physics and Applications of Non-Crystalline Semiconductors in Optoelectronics* (Kluwer Academic, Dordrecht, 1997)
21. I. Blonskyi, V. Kadan, O. Shpotyuk, I. Dmytruk, Opt. Commun. **282**, 1913 (2009)
22. I. Blonskyi, M. Brodyn, V. Kadan, O. Shpotyuk, I. Dmitruk, I. Pavlov, Appl. Phys. B **97**, 829 (2009)
23. J.M. Saiter, M. Arnoult, J. Grenet, Physica B **335**, 370 (2005)
24. P. Lucas, A. Doraiswamy, E.A. King, J. Non-Cryst. Solids **332**, 35 (2003)
25. P. Lucas, E.A. King, A. Doraiswamy, P. Jivaganont, Phys. Rev. B **71**, 104207 (2005)
26. H. Fritzsche, Semiconductors+ **32**, 850 (1998)
27. D. Marcuse, Appl. Opt. **18**, 9 (1979)
28. W. Merzkirch, *Flow Visualization* (Academic Press, New York, 1987)
29. R. de Bruyn, E. Bodenschatz, S.W. Morris, S.P. Trainoff, Y. Hu, D.S. Cannel, G. Ahlers, Rev. Sci. Instrum. **67**, 2043 (1996)
30. A. Gopal, S. Minardi, M. Tatarakis, Opt. Lett. **32**, 1238 (2007)
31. E. Ampem-Lassen, S.T. Huntington, N.M. Dragomir, K.A. Nugent, A. Roberts, Opt. Express **13**, 3277 (2005)